A multiscale approach for BTJ-VCSEL electro-optical analysis

Alberto Gullino*, Simone Pecora*, Alberto Tibaldi*†, Francesco Bertazzi*†,
Michele Goano*†, and Pierluigi Debernardi†
* Dipartimento di Elettronica e Telecomunicazioni, Politecnico di Torino, Corso Duca degli Abruzzi 24, 10129 Torino, Italy
† CNR-IEIIT, Corso Duca degli Abruzzi 24, 10129 Torino, Italy
E-mail: alberto.tibaldi@polito.it

***Abstract*—This paper presents a theoretical comparison of the electro-optical characteristics of 850 nm GaAs/AlGaAs *pin*- and BTJ-based VCSELs. The calculations are based on a drift-diffusion model coupled with a NEGF formalism, able to model accurately the tunneling across the TJ. The resulting *LIV* characteristics demonstrate promising improvements, at both 25 and 80 °C, enabled by TJ confinement scheme.**

I. Introduction

Most vertical-cavity surface-emitting lasers (VCSELs) are based on *pin* devices emitting in the near-IR (850–980 nm) [1]. In these devices, optical and electrical confinement is realized with an oxide aperture, achieved by a wet oxidation of a thin AlAs layer. In all the other wavelength windows, ranging from 1.3–2.6 μm (InP-based [2]) to 2.3–3.0 μm (GaSb-based [3]) or even 4 μm [4], the confinement is achieved by the technological-enabler buried tunnel junction (BTJ) concept. BTJs are based on more controllable etching steps, which allow precise definitions of the active region. BTJ-VCSELs do not require the highly resistive and absorbing p-doped distributed Bragg reflectors (DBRs), which can be replaced with n-doped layers, thus limiting free-carrier absorption (FCA) losses and self-heating [5].

The chance to get rid of the hardly-controllable wet oxidation step and of p-doped layers, hence enabling low-resistance paths to a well-defined active region, is interesting also for GaAs VCSELs. In order to demonstrate the benefits of BTJ-VCSELs, the scope of this paper is to present a first comparative study with an equivalent *pin* device. Aiming to minimize on-wafer prototypes, this work is based on our in-house 1D drift-diffusion simulator D1ANA (drift-diffusion 1D-ANAlysis) [6], coupled self-consistently with a nonequilibrium Green's function (NEGF) formalism describing rigorously the quantum tunneling in the TJ region [7]. Optical simulations are based on our in-house electromagnetic simulator VELM [8], [9].

II. Results and outlooks

The two VCSELs under investigation feature a 1λ-cavity embedding three 8 nm GaAs quantum wells (QWs), defined by a couple of distributed Bragg reflectors (DBRs). The bottom n-DBR is made of 36 pairs, while the top DBR is designed to achieve similar optical threshold gains in the two VCSELs. This results in 21 pairs (p-doped) for the oxide-confined device and 19 (n-doped) for the BTJ-VCSEL, taking advantage of the lower FCA in the n-doped mirror in the latter device [5]. DBRs are composition- and doping-graded to improve carrier transport and minimize FCA losses. Both structures lie on a 110 μm thick n-type GaAs substrate.

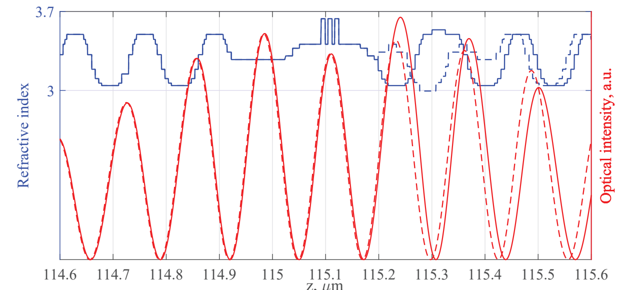

Fig. 1: Refractive index (in blue) and standing wave (in red, from VELM) for the two VCSELs: continuous lines - TJ; dashed - oxide confined. Ground contact is placed at $z = 0$ μm, output light is emitted at the right hand side ($\lambda = 847.7$ nm and $G_{th} = 1480$ cm^{-1} for the TJ-VCSEL; $\lambda = 847.9$ nm, $G_{th} = 1440$ cm^{-1} for the oxide confined).

In Fig. 1, the blue curves show the refractive index of both devices in the proximity of the cavity, whereas red curves represent the corresponding standing waves. The most apparent difference concerns the layers right after the cavity, where the oxide aperture is replaced by the BTJ and an electron-blocking layer (p-doped, with the same composition of a DBR pair) is introduced to reduce carrier leakage from the TJ itself [7]. This results in a 5 nm shift with respect to the oxide-confined VCSEL, required to place the highly doped TJ in a node of the optical field. The central peak is correctly centered in the MQW region to achieve the maximum interaction between gain and optical field.

D1ANA is based on the drift-diffusion (DD) model [10], thus it solves in a self-consistent fashion the Poisson's equation with the carrier continuity equations. Fermi-Dirac statistics is used to describe electron and hole densities, together with an incomplete ionization model of the dopants. Quantum corrections are adopted to model properly the active region containing QWs [11], [12]. This is accomplished by introducing 2D and 3D active region carrier populations and coupling them through a capture time. Optical data, such as modal losses, optical confinement factor and output power coupling coefficient, are extracted from VELM, and plugged

978-1-6654-1276-6/21/$31.00 ©2021 IEEE

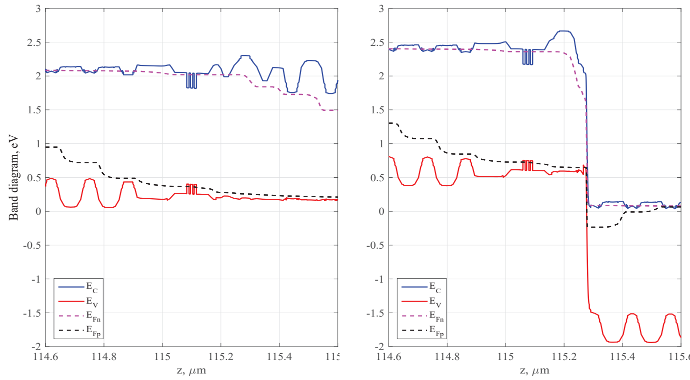

Fig. 2: Band diagram at 25°C of oxide-confined VCSEL (left) and BTJ-VCSEL (right), at 3 V.

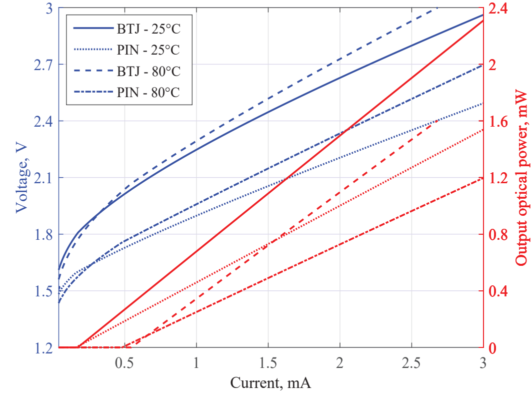

Fig. 3: LIV curves of TJ and oxide-confined VCSELs at room temperature and at 80° C.

in D1ANA to describe coupling between carriers and photons. The gain model is based on Fermi's golden rule, where the electronic band structure is described with the Luttinger-Kohn Hamiltonian [13].

Following the approach presented in [7], self-consistency between DD solver and NEGF formalism is achieved by extracting from NEGF a generation term accounting for the tunneling inside the TJ in reverse bias condition, and introducing it in the bulk layers treated with semiclassical DD model alongside GR rates induced by Auger, SRH and radiative recombination. This is carried out by applying NEGF to the TJ region (less than 20 nm long), therefore heavily reducing the computational burden of the overall simulation.

Fig. 2 shows the band diagrams at 3 V of both devices at room temperature. While in the oxide-confined VCSEL (left hand side figure) carrier injection into the cavity is provided by transport across the oppositely doped DBRs, in the BTJ-VCSEL (right hand side figure) hole injection relies on quantum transport in the tunneling region. This entails significant differences between band diagrams. From the electrical standpoint, the oxide-confined VCSEL behaves as a pin junction in forward bias. Conversely, BTJ-VCSEL embeds a heavily doped TJ in counterseries with the cavity (n-i-p-p^+n^+-n). As a consequence, voltage drop across the TJ is significantly smaller than the applied bias [7], *e.g.*, at 3 V it is smaller than 0.6 V.

Fig. 3 reports electrical and optical results at room temperature and at 80° C. Connection between D1ANA and our 3D VCSEL suite is obtained by including a fitting "size factor", accounting for the neglected radial features [14]. BTJ-VCSEL IV curves (in blue) display lower currents at equal applied bias than the oxide-confined device, at both temperatures. This is a direct consequence of the aforementioned relative position of the junctions: a significant current starts to flow across the device when both junctions enter into a significant conduction condition [7].

This small electrical penalty is overcome by the improvements of the optical performance (in red), where BTJ-VCSEL reaches higher output optical power at equal current values. The removal of almost all the p-doped layers in the BTJ-VCSEL leads to a reduction of losses, so the slope of the corresponding LI curves is significantly higher. As imposed by the similar optical threshold gains, the threshold currents of the two VCSELs stay pretty similar at both temperatures.

Future works will be directed towards the inclusion of a proper thermal solver, self-consistent with the electro-optical used here. As soon as such a multiphysics 1D solver is realized, we want to extend our Vcsel Electro-opto-thermal NUmerical Simulator VENUS with this novel approach to accurately model BTJ-VCSELs.

References

[1] R. Michalzik, ed., *VCSELs: Fundamentals, Technology and Applications of Vertical-Cavity Surface-Emitting Lasers* (Springer-Verlag, Berlin, 2013).
[2] V. Iakovlev, *et al.*, *IEEE Photon. Technol. Lett.* **17**, 947 (2005).
[3] A. Bachmann, K. Kashani-Shirazi, S. Arafin, M.-C. Amann, *IEEE J. Select. Topics Quantum Electron.* **15**, 933 (2009).
[4] G. K. Veerabathran, S. Sprengel, A. Andrejew, M.-C. Amann, *Appl. Phys. Lett.* **110**, 071104 (2017).
[5] P. Debernardi, *et al.*, *IEEE J. Select. Topics Quantum Electron.* **25**, 1700914 (2019).
[6] M. Calciati, A. Tibaldi, F. Bertazzi, M. Goano, P. Debernardi, *Semiconductor Sci. Technol.* **32**, 055007 (2017).
[7] A. Tibaldi, *et al.*, *Phys. Rev. Appl.* **14**, 024037 (2020).
[8] G. P. Bava, P. Debernardi, L. Fratta, *Phys. Rev. A* **63**, 23816 (2001).
[9] P. Debernardi, G. P. Bava, *IEEE J. Select. Topics Quantum Electron.* **9**, 905 (2003).
[10] F. Bertazzi, *et al.*, *Handbook of Optoelectronic Device Modeling and Simulation*, J. Piprek, ed. (CRC Press, Boca Raton, FL, 2017), chap. 2, pp. 35–80.
[11] M. Grupen, K. Hess, *IEEE J. Quantum Electron.* **34**, 120 (1998).
[12] A. P. Cédola, *et al.*, *Int. J. Photoenergy* **2018**, 7215843 (2018).
[13] S. L. Chuang, *Physics of Photonic Devices* (John Wiley & Sons, Hoboken, 2009).
[14] A. Gullino, *et al.*, *20th International Conference on Numerical Simulation of Optoelectronic Devices (NUSOD 2020)* (online, 2020), pp. 65–66.